Int. J. Electrochem. Sci., 13 **(2018)** 6229 – 6235, doi: 10.20964/2018.07.31

International Journal of
ELECTROCHEMICAL
SCIENCE
www.electrochemsci.org

Short Communication

Mesoporous TiO_2 Spheres/Graphene Composite as a High-Performance Anode Material for Lithium-ion Batteries

Tianyu Du[1], *Weixing Zhang*[1,*], *Han Peng*[2,*], *Gaurav Jain*[3]

[1] College of Chemical and Biological Engineering, Zhejiang University 310027 PR China
[2] School of Mechanical Engineering, North China University of Water Resources and Hydropower, Zhengzhou, Henan Province
[3] Medtronic Energy and Component Center, Brooklyn Center, USA
[*]E-mail: 21428079@zju.edu.cn hanpeng008@tom.com

Received: 1 April 2018 / *Accepted:* 8 May 2018 / *Published:* 5 June 2018

Mesoporous TiO_2 spheres/graphene (TOS/G) composites were successfully prepared via a UV-assisted method of reduced graphene oxide with hydrazine. The as-prepared TOS/G composites exhibit a high initial discharge capacity of 218 mAh g^{-1} and retain 86% of reversible capacity over 100 cycles at a rate of 0.2 C.

Keywords: TiO_2 sphere, graphene, anode, lithium-ion battery.

1. INTRODUCTION

Improving renewable and sustainable energy has become a very important issue in the rapid development of society due to the rapidly fading fossil energy resources and acute environmental pollution with sudden climate change. Therefore, it is imperative to develop a new type of energy system for the governments and scientists around the world. Lithium-ion batteries have attracted considerable attention due to their high energy density, long cycle life and environmental friendliness. As is well known, the anode materials have a significant effect on the performance of lithium-ion batteries[1, 2, 3]. Therefore, numerous efforts by research groups have been made to develop high-performance anode materials such as TiO_2 and TiO_2-based materials during the past few decades. However, many problems have hindered the application of TiO_2 electrode materials during the industrialization process. It is known that one of the major challenges is capacity fading caused by severe aggregation during the charge-discharge processes and poor electronic conductivity [4-9].

Consequently, the key factors to improve the performance of lithium-ion batteries include restraining the aggregation of TiO_2 and enhancing the electronic conductivity of the anode. To suppress

the volume changes and aggregation of TiO_2, a variety of methods have been applied that involve the design of TiO_2 with various nanostructures such as TiO_2 nanoparticles [10, 11], spheres [12, 13] and nanofibers [14].

In this work, mesoporous TiO_2 spheres/graphene (TOS/G) composites have been successfully synthesized via a UV-assisted method of reduced graphene oxide with hydrazine. The as-prepared TOS/G composites exhibit excellent electrochemical performance.

2. EXPERIMENTAL

2.1 Preparation of the mesoporous TiO_2 spheres

Typically, 5.0 mL of titanium isopropoxide (TIP) was added into 16 mL of ethanol and 10 mL of a deionized water mixture with an ammonia concentration of 0.12 M under magnetic stirring. Then, the solution was transferred into a PTFE tank and heated at 160°C for 16 h. After cooling down to room temperature, the powder was washed with ethanol and dried at 60°C for 24 h. Finally, the mesoporous TiO_2 spheres were obtained.

2.2 Preparation of the TOS/G composite

Thirty milligrams of graphite oxide and 45 mg of TiO_2 were dissolved in 50 mL deionized water under ultrasonication for 2 h. Then, 100 ml N_2H_4•H_2O was added into the above solution under UV illumination. After cooling to room temperature, the products were collected to obtain the TOS/G composites.

2.3 Material characterization

The as-obtained samples were characterized by using a scanning electron microscope (SEM, JSM-7001F), transmission electron microscope (TEM, Tecnai F20), an X-ray diffractometer (XRD, D8 Advance, BRUKER). The content of graphene in the TOS/G composite was determined by thermogravimetric analysis (TG, TA Q600 instrument).

2.4 Electrochemical measurements

The electrochemical performance was measured by using coin-type (CR2016) half batteries. A slurry was prepared by mixing 80 wt.% samples, 10 wt.% acetylene black and 10 wt.% PVDF with NMP. Then, the slurry was uniformly casted onto a Cu foil with a doctor blade to prepare a film-type electrode. The electrode was dried for 12 h under vacuum at 120°C and was cut into circular electrodes. The cells were assembled in an Ar-filled glove box with lithium foil as both the reference and counter electrode, and a solution of 1.0 M LiPF6 was dissolved in 1:1 (v/v) EC/DEC as the

electrolyte. All electrochemical measurements were carried out on a battery testing system (LAND CT 2001A) in the potential range from 0.01 V to 3 V. Electrochemical impedance spectroscopy (EIS) was conducted on an electrochemistry workstation in the frequency range from 100 kHz to 0.01 Hz.

3. RESULTS AND DISCUSSION

3.1 Materials Characterization

As shown in Fig. 1a, TiO_2 exhibits a 3D sphere structure with diameter of 100-150 nm. In addition, the surface of the TiO_2 spheres are rough and composed of large amounts of nanoparticles, which enhance the contact area between the electrolyte and electrode material. Fig. 1b shows the morphology of the TiO_2/graphene composite. The graphene uniformly dispersed on the TiO_2 spheres produce an interconnected structure, which provides a path for the transportation of electrons. Fig. 1c shows the TEM image of the TiO_2/graphene composite. It can be observed that the TiO_2 spheres are surrounded by graphene sheets. Fig. 1d is a high-resolution TEM image of the TiO_2/graphene composite. This image clearly displays the TiO_2 crystals with sizes of 10 nm, and the interface spacing is 0.35 nm, which is accord with the (101) plane of the anatase phase [15].

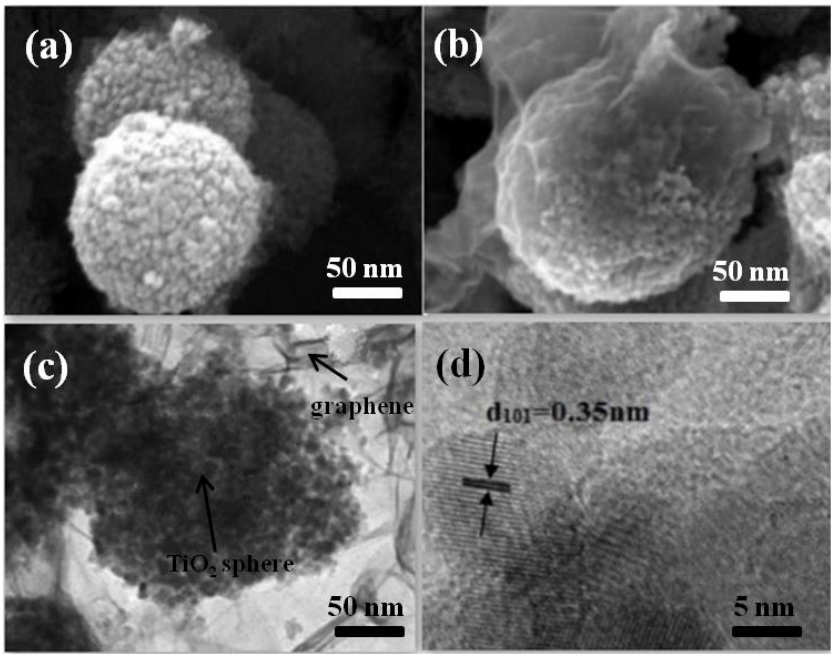

Figure 1. SEM images of the (a) TOS and (b) TOS/G composite; (c) TEM image of the TOS/G composite; and (d) HRTEM image of the TOS/G composite.

Fig. 2 shows the XRD patterns of TiO_2 and TiO_2/graphene. As shown in Fig. 2, good crystalline TiO_2 spheres were successfully synthesized without any clutter, indicating the purity of the as-prepared TiO_2 spheres. The characteristic diffraction peaks can be indexed into the (101), (103), (004), (112), (200), (105), (211), (213), (204), (116), (220) and (215) planes of anatase TiO_2 (JCPDS card No. 21-

1272) [16]. Notably, the characteristic peak of graphene at 26°C is not observed in the TiO_2/graphene composite. This phenomenon is caused by the coincidence of the TiO_2 spheres and graphene. The reason is that the characteristic peak of graphene (002) overlaps with the characteristic peak of TiO_2 (101) [17].

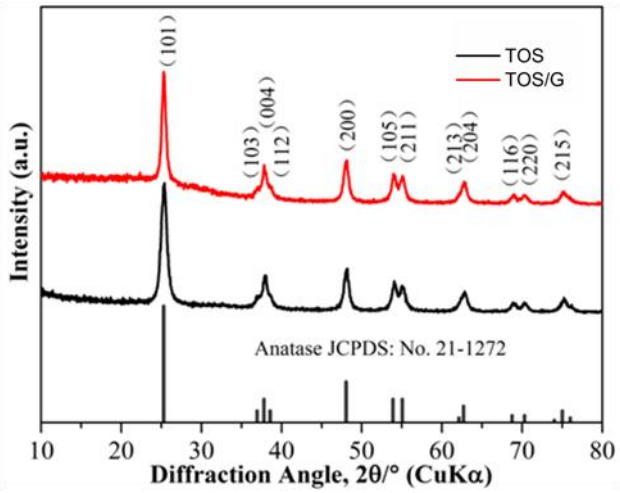

Figure 2. XRD patterns of the TOS and TOS/G composite.

Fig. 3 is the TG curve of the TiO_2/graphene composite. The weight loss below 100°C is due to the evaporation of water in the composite material, and the weight loss in the range of 100-600°C is derived from the decomposition of graphene. It can be concluded that the content of graphene is approximately 2.4% in the TiO_2/graphene composite.

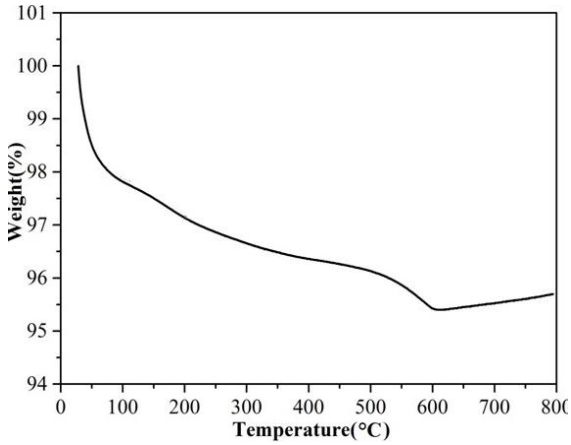

Figure 3. TGA profile of the TOS/G composite.

3.2 Electrochemical performance

Fig. 4a shows the initial discharge-charge profiles of the TiO_2 spheres and TiO_2/graphene composite between 1.0-3 V at a current density of 0.2 C. It can clearly be seen that charging and discharging platforms are located at 1.5/1.9 V, which represents the process of the insertion/extraction

of Li^+ in the TiO_2 spheres. The lithium storage mechanism of the TiO_2 spheres can be described by the reaction below:

$$TiO_2 + xLi + + xe^- \rightarrow Li_xTiO_2$$

The first discharge and charge capacities of the TiO_2/graphene composite are 276 mAh g^{-1} and 218 mAh g^{-1}, respectively, with a coulombic efficiency of approximately 79%. It is suggested that the TiO_2/graphene composite microspheres have better reversibility during the first charge and discharge process. However, the first discharge and charge capacity of the TiO_2 sphere are 228 mAh g^{-1} and 310 mAh g^{-1}. The coulombic efficiency is only 72.2%.

The comparison of rate performances for the TiO_2 spheres and TiO_2/graphene composite is shown in Fig. 4b. Despite a certain capacity decay at 0.1 C, the two samples show a stable capacity value under the subsequent large current densities. When the current density increases to more than 0.2 C, the capacity of the TiO_2/graphene composite becomes higher than that of pure TiO_2. In addition, when the current density returns to 0.1 C, the reversible capacity of the TiO_2/graphene composite remains at 198 mAh g^{-1}, and the capacity retention is 85%. However, the reversible capacity of TiO_2 is 188 mAh g^{-1} with capacity retention of only 78%. This result indicates that the TiO_2/graphene composite demonstrates more excellent rate performance. This excellent rate performance is attributed to the hybrid structure of the TOS/G composite, which could restrain the aggregation and improve the electronic conductivity of the TiO_2 spheres at the same time.

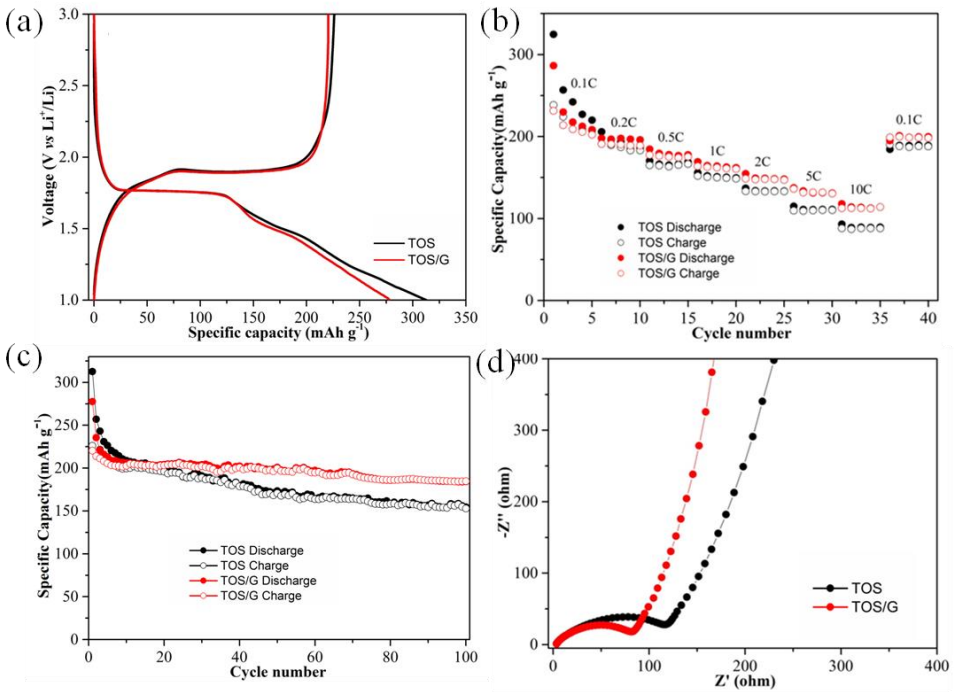

Figure 4. (a) Initial charge-discharge profiles of the TOS and TOS/G composite at 0.2 C; (b) Rate performance of the TOS and TOS/G composite at various current densities; (c) Cycle performance of the TOS and TOS/G composite at 0.2 C; and (d) Nyquist plots of the TOS and TOS/G composite.

Fig. 4c shows the cycle performances of the TiO_2 spheres and TiO_2/graphene composite at a current density of 0.2 C. The specific capacity of TiO_2/graphene is maintained at 218 mAh g^{-1} after 100 cycles, while the capacity retention rate is 86%. However, the specific capacity and capacity retention rate of the TiO_2 sphere is only 155 mAh g^{-1} and 69%, respectively, after 100 cycles, which are much lower than those of the TiO_2/graphene composite. Clearly, the cycle performance of the TOS/G composite is better than that of the pure TiO_2 spheres. This finding demonstrates that the structure of the TOS/G composites is stable during the charge/discharge process.

To further investigate the influence of graphene on TiO_2, EIS measurements were conducted. As shown in the Nyquist plots (Fig. 4d), the radius of the TiO_2/ graphene composite in the high-frequency region is smaller than that of the TiO_2 spheres, indicating a smaller contact impedance between the electrolyte and the electrode material and the charge transfer resistance, which demonstrates that graphene can effectively improve the Li^+ diffusion rate at the electrode surface. In addition, in the low-frequency region, the slope of the TiO_2/graphene composite is steeper, indicating a smaller Warburg impedance. Consequently, the TOS/G composites exhibit superior electronic conductivity.

Furthermore, to demonstrate the excellent electrochemical performance of the TOS/G composite, the comparison of electrochemical performance for similar anode materials is listed in Table 1. It can be seen that the TOS/G composites exhibit stable cycle performance among these reported anode materials for lithium-ion batteries.

Table 1 The comparison of various anode materials for LIBS.

Materials	Current densities (C)	Capacity (cycle number)	Reference
TOS/G	0.2	218 (100)	This work
TiO_2 spheres	0.2	208 (100)	18
TiO_2@C	0.2	142(100)	19

4. CONCLUSIONS

In conclusion, mesoporous TiO_2 spheres/graphene (TOS/G) composites have been successfully synthesized via a UV-assisted method of reduced graphene oxide with hydrazine. The as-prepared TOS/G composites exhibit a high initial discharge capacity of 218 mAh g^{-1} and retain 86% of reversible capacity over 100 cycles at a rate of 0.2 C.

References

1. N. J. Song and C. L. Ma, *Int. J. Electrochem. Sci.*, 13 (2018) 452.
2. X. L. Tong, M. Zeng, J. Li and F. Y. Li, *Appl. Surf. Sci.*, 392 (2017) 897.
3. I. Nam, N.D. Kim, G.P. Kim, J. Park and J. Yi, *J. Power Sources*, 244 (2013) 56.

4. W. Tang, Y. Hou, F. Wang, L. Liu, Y. Wu and K. Zhu, *Nano lett.*, 13 (2013) 2036.
5. Q. H. Tian, L. X. Li, J. Z. Chen, L. Yang and S. I. Hirano, *J. Power Sources*, 376 (2018) 1.
6. L. Y. Zheng, X. Y. Wang, Y. G. Xia, S. L. Xia and Y. J. Cheng, *ACS Appl. Mater. Interfaces*, 10 (2018) 2591.
7. W. Zhang, Y. Zeng, N. Xiao, H.H. Hng and Q. Yan, *J. Mater. Chem.*, 22(2012) 8455.
8. H. Chen, H. Liu, Y. Guo, B. Y. Wang and H. Wu, *J. Alloy. Compd.*, 731 (2018) 844.
9. J. J. Ren, L. W. Su, X. Qin, M. Yang, J. P. Wei, Z. Zhou and P. W. Shen, *J. Power Sources*, 264 (2014) 108.
10. L. T. Yan, J. L. Yu and H. M. Luo, *Appl. Mater. Today*, 8 (2017) 31.
11. Y. C. Yang, W. Shi, S. J. Liao, R. H. Zhang and S. L. Leng, *J. Alloy. Compd.*, 746 (2018) 619.
12. T. L. Ding, J. X. Wu, Z. L. Chen, T. B. Lan and M. D. Wei, *J.Electroanal Chem.*, 818 (2018) 1.
13. Y. Cai, H. E. Wang, J. Jin, S. Z. Huang, Y. Yu, Y. Li, S. P. Feng and B. L. Su, *Chem. Eng. J*, 281 (2015) 844.
14. H. Chen, H. Liu, Y. Guo, B. Y. Wang, Y. H. Wei, Y. Zhang and H. Wu, *J. Alloy. Compd.*, 731 (2018) 844.
15. Y. L. Ding, J. A. Xie, G. S. Cao, T. J. Zhu, H. M. Yu and X. B. Zhao, *Adv. Funct. Mater.*, 21 (2011) 348.
16. H. Huang, J. G. Yu, Y. P. Gan and Y. Xia, Mater. Res. Bull., 96 (2017) 425.
17. D. Zhan, Q. G. Zhang, X. H. Hu, G. Z. Zhu and T. Y. Peng, *Solid State Ionics*, 239 (2013) 8.
18. J. Q. Wang, Y. J. Huang, M. Zeng and R. F. Peng, *Mater. Lett.*, 181 (2016) 289.
19. L. Tan, L. Pan, C. Y. Cao, B. F. Wang and L. Li, *J. Power Sources*, 253 (2014) 193.